

Robot Control for Simultaneous Impact Tasks through Time-Invariant Reference Spreading

Jari J. van Steen, Nathan van de Wouw and Alessandro Saccon

Abstract—With the goal of enabling the exploitation of impacts in robotic manipulation, a new framework is presented for control of robotic manipulators that are tasked to execute nominally simultaneous impacts. In this framework, we employ tracking of time-invariant reference vector fields corresponding to the ante- and post-impact motion, increasing its applicability over similar conventional tracking control approaches. The ante- and post-impact references are coupled through a rigid impact map, and are extended to overlap around the area where the impact is expected to take place, such that the reference corresponding to the actual contact state of the robot can always be followed. As a sequence of impacts at the different contact points will typically occur, resulting in uncertainty of the contact mode and unreliable velocity measurements, a new interim control mode catered towards time-invariant references is formulated. In this mode, a position feedback signal is derived from the ante-impact velocity reference, which is used to enforce sustained contact in all contact points without using velocity feedback. With an eye towards real implementation, the approach is formulated using a QP control framework, and is validated using numerical simulations both on a rigid robot with a hard inelastic contact model and on a realistic robot model with flexible joints and compliant partially elastic contact model.

I. INTRODUCTION

Exploitation of intentional impacts plays a vital role in increasing the versatility and efficiency of robots for a range of applications in locomotion and manipulation. In locomotion, such intentional impacts enable humanoid running [1], while for manipulation, utilizing intentional impacts can ensure a faster and more energy-efficient handling of objects [2], which increases the applicability of robots in an industrial setting. While exploiting impacts is part of the repertoire of human skills, seen in applications like running or kicking a ball, such impacts can cause issues when translated to applications in robotics. Clearly, hardware can break when impact forces are too high. But even when impacts stay within safe limits such that no damage occurs, the rapid velocity transitions that result from the impact can result in performance and stability issues when controlling the robot if not accounted for. An example of the latter is the peak in the error between the desired and actual velocity of the robot under tracking control, which appears as a result of the inevitable mismatch in time between the expected velocity jump in the reference, and the actual velocity jump [3], [4].

This work will focus specifically on what we call nominally simultaneous impacts, which take place when multiple points between the robot and its environment are tasked to simultaneously come into contact at non-zero speed. An example of an application that shows such behavior is dual arm industrial robots swiftly grabbing boxes [5]. As the impacting

surfaces are unlikely to be perfectly aligned at the time of impact, a series of spurious impacts will typically occur instead of the planned nominal simultaneous impact. As a result, the system will experience an unpredictable series of velocity jumps, and pass through a series of uncertain contact states before full contact is established. As we will show, this implies that velocity feedback control cannot be reliably used during an impact sequence.

In recent years, a few control methods have been developed to accurately execute motions that include simultaneous impacts while avoiding unwanted spikes in the control inputs. This includes tracking approaches such as [6], [7], and the framework of reference spreading, introduced in [8] and expanded upon in [9], [10], [11]. Reference spreading is a hybrid control approach that deals with impacts by defining ante- and post-impact references that overlap around the nominal impact time. It is ensured that the reference used for tracking control corresponds with the actual contact state of the robot by switching the reference based on detection of the impact, which avoids error peaking and related spikes in the control inputs. At the nominal impact time, the ante- and post-impact references are coupled by an impact map such that the tracking error is ideally zero if the nominal motion were to be tracked exactly. While initially defined solely for single impacts, reference spreading has been shown to lend itself for tracking control for scenarios with inelastic simultaneous impacts in [12], [13]. This is achieved by including an additional interim control mode, which is active from the moment of the first impact until full contact is established. In this mode, velocity error feedback is turned off due to the uncertainty of the contact state.

All of the aforementioned approaches rely on tracking control of trajectories that are defined explicitly as a function of time. While this can be used to accurately execute desired motions and make impacts with a given desired velocity at a desired time, it is not necessarily an ideal strategy for all applications [14], [15]. If collision avoidance, conflicting tasks or an unexpected disturbance cause the robot to lag behind the nominal motion, it is generally undesirable to force the robot back to a trajectory prescribed in time. Additionally, it is desirable to prescribe a task in a way that is robust to variations in the initial conditions, such that it is not required to re-plan a trajectory when the initial robot pose is altered.

A time-invariant control approach, where the robot follows a certain desired velocity reference based on its current posture, such as [16], would be more suitable for such scenarios. However, time-invariant control schemes that deal

with motions containing (simultaneous) impacts are limited. State-of-the-art time-invariant robot control approaches such as [17] focus on impact avoidance rather than exploitation of impacts. Previous works have focused on using learned time-invariant references to hit objects with nonzero velocity [18], [19]. However, potential stability or performance issues after the impact are not explicitly addressed in these works.

The contribution in this paper is the formulation of an approach based on time-invariant reference velocity and force fields, used for control of mechanical systems tasked to perform nominally simultaneous inelastic impacts. The proposed controller has a switching structure that resembles the tracking controller proposed in [13], which consists of an ante-impact, interim, and post-impact control mode based on the aforementioned reference spreading paradigm. While [13] relies on position feedback in this interim mode, here, a new approach based on integration of the velocity references over time is used due to the lack of an explicit position reference when using these reference fields. Furthermore, we show that the new time-invariant approach can be cast into the quadratic programming (QP) robot control framework [20], [21], [22], allowing to include additional constraints ensuring for example collision avoidance and adherence to joint limits, which are essential in real applications. Impact-aware QP control is an active area of research [23], [24], and this paper contributes also to that line of research.

The structure of this paper is as follows. In Section II, we will provide the equations of motion of the 3DOF robot that we will use to demonstrate the proposed control approach. In Section III, the generation of the ante- and post-impact reference velocity fields is described. Section IV presents the control framework consisting of the ante-, interim-, and post-impact modes, used to track these references. In Section V, we validate the approach against two other baseline methods by means of numerical simulations, before drawing conclusions in Section VI.

II. ROBOT DYNAMICS

While the control strategy described in this paper can be applied to a wider range of scenarios, the planar manipulator depicted in Figure 1, which is identical to the manipulator used throughout [13], is used in this paper to illustrate and demonstrate the approach. The robot consists of three rigid frictionless actuated joints and rigid links, and impacts a hinged rigid plank. The system's generalized coordinate vector is $\mathbf{q} = [\mathbf{q}_{\text{rob}}^T q_4]^T$ with $\mathbf{q}_{\text{rob}} = [q_1 \ q_2 \ q_3]^T$. The mass of each link i and its inertia around the center of gravity are given by m_i and $I_{g,i}$ respectively, with the inertia of the plank around the hinge given by $I_{o,4}$. The vector normal to the plank is described by \mathbf{n} . The end effector position \mathbf{p} and orientation θ describe the position and orientation of frame $o_e x_e y_e$ expressed in terms of frame $o_0 x_0 y_0$, with their respective velocities given by

$$\dot{\mathbf{p}} = \mathbf{J}_p(\mathbf{q})\dot{\mathbf{q}}, \quad \dot{\theta} = \mathbf{J}_\theta(\mathbf{q})\dot{\mathbf{q}}. \quad (1)$$

with $\mathbf{J}_p(\mathbf{q}) = [\mathbf{J}_{p,\text{rob}}(\mathbf{q}) \ 0]$, $\mathbf{J}_\theta(\mathbf{q}) = [\mathbf{J}_{\theta,\text{rob}}(\mathbf{q}) \ 0]$, and

$$\mathbf{J}_{p,\text{rob}}(\mathbf{q}) = \frac{\partial \mathbf{p}}{\partial \mathbf{q}_{\text{rob}}}, \quad \mathbf{J}_{\theta,\text{rob}}(\mathbf{q}) = \frac{\partial \theta}{\partial \mathbf{q}_{\text{rob}}},$$

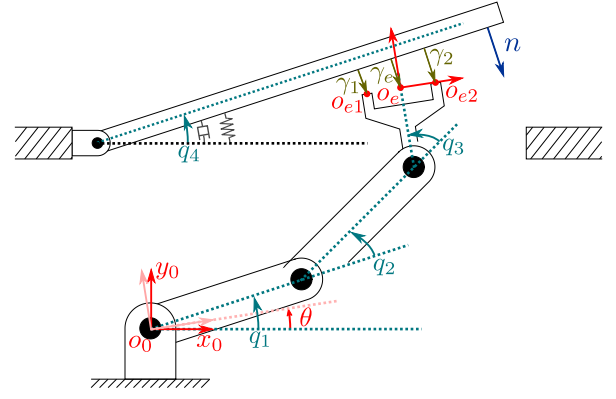


Fig. 1: Overview of the 3DOF planar manipulator impacting a hinged rigid plank.

For ease of notation, in the following we will drop the explicit dependency on \mathbf{q} (or $\dot{\mathbf{q}}$). The contact between the end effector and the plank can occur at two distinct point as shown in Figure 1, and is assumed to be frictionless. These contacts can be described by the gap functions γ_i and corresponding contact forces λ_i , for $i \in \{1, 2\}$, satisfying the complementarity conditions

$$0 \leq \gamma_i \perp \lambda_i \geq 0, \quad (2)$$

which is a common description in the framework of nonsmooth mechanics [25]. This implies that the contact force is zero when the contact is open and non-negative when the contact is closed.

A. Non-impulsive free and constrained dynamics

The robot dynamics in free and constrained motion are

$$\mathbf{M}\ddot{\mathbf{q}} + \mathbf{h} = \mathbf{S}\boldsymbol{\tau} + \mathbf{J}_N^T \boldsymbol{\lambda}, \quad (3)$$

with joint positions \mathbf{q} , mass matrix \mathbf{M} , vector of gravity, centrifugal, and Coriolis terms \mathbf{h} , applied joint torques $\boldsymbol{\tau}$, actuation matrix $\mathbf{S} = [\mathbf{I}_{3 \times 3} \ 0_3]^T$, and normal contact forces $\boldsymbol{\lambda}$ (being zero in free motion). The contact Jacobian is given by $\mathbf{J}_N = [\mathbf{J}_{N,1}^T \ \mathbf{J}_{N,2}^T]^T$, with

$$\mathbf{J}_{N,i} = \frac{\partial \gamma_i}{\partial \mathbf{q}}. \quad (4)$$

B. Impulsive impact dynamics

To ensure adherence to the non-penetration condition $\gamma_i \geq 0$ appearing in (2), an instantaneous jump in $\dot{\mathbf{q}}$ has to be allowed as soon as a contact is closed. This state-dependent jump is described by a so-called impact map [26]. This results in a potential discontinuity in joint velocities at the impact time, with ante-impact velocity $\dot{\mathbf{q}}^-$, post-impact velocity $\dot{\mathbf{q}}^+$, and continuous position $\mathbf{q}^- = \mathbf{q}^+$. Integrating (3) over the impact time with λ allowed to become impulsive, leads to the impact equation [25] given by

$$\mathbf{M}(\dot{\mathbf{q}}^+ - \dot{\mathbf{q}}^-) = \mathbf{J}_N^T \boldsymbol{\Lambda}, \quad (5)$$

with $\boldsymbol{\Lambda}$ the momentum associated to the impulsive contact forces. We assume inelastic impacts to take place at the moment of contact transition, which means we assume that

the impact law is given by $\dot{\gamma}_i^+ = 0$. This means that, when contact of the end effector with the plank is established simultaneously at both possible contact locations, we have

$$J_N \dot{q}^+ = 0. \quad (6)$$

Combining (5) and (6) leads to the simultaneous impact map

$$\dot{q}^+ = \left(I - M^{-1} J_N^T (J_N M^{-1} J_N^T)^{-1} J_N \right) \dot{q}^-. \quad (7)$$

The inelastic impact map will be used in the formulation of the reference velocity fields in the next section.

III. DESIRED PATH GENERATION

In this section, we will give details on the design of the time-invariant ante-impact and post-impact reference velocity fields as a function of the end-effector pose, which we use in the control law in Section IV to execute the desired motion. Ideally, when perfectly followed, this reference should guarantee a simultaneous impact, with zero velocity tracking error before and after the state jump.

A. Ante-impact

The process of generating the desired ante-impact reference velocity can be decoupled into two parts, the first being a reference to guide the end effector position towards the hinged plank with a given velocity denoted by $\bar{p}_d^a(p)$, and the second being an orientation reference $\dot{\theta}_d^a(\theta)$ to align the orientation of the end effector with that of the hinged plank to pursue a simultaneous impact. Both references are time-invariant, and depend solely on the state of the manipulator.

1) *Position*: The ante-impact linear velocity reference $\bar{p}_d^a(p)$ is formulated with the goal of guiding the end effector towards the line or area where the desired impact is expected to take place, which is defined as the *nominal impact line* for our use case. In the use case of Figure 1, this nominal impact line is given by the bottom of the plank with the plank in a fixed a priori estimated state at the time of impact, given by $q_{4,\text{est}}^-$. We have taken $q_{4,\text{est}}^- = \dot{q}_{4,\text{est}}^- = 0$, corresponding to the equilibrium position of the hinged plank.

We define $d : \mathbb{R}^2 \rightarrow \mathbb{R}, p \mapsto d(p)$ as the smallest distance from the point p to this nominal impact line, as shown in Figure 2. With this, the first step to formulate $\bar{p}_d^a(p)$ is the formulation of a velocity reference $\dot{p}_d^a(p)$ for all end effector positions p that lie before the nominal impact line, corresponding to $d(p) < 0$, which is formulated in Appendix A. In line with the core idea of reference spreading, we extend this reference past the nominal impact line to formulate the extended velocity reference given by

$$\bar{p}_d^a(p) = \begin{cases} \dot{p}_d^a(p) & \text{if } d(p) \leq 0, \\ \dot{p}_d^a(p + d(p)n_{\text{imp}}) & \text{if } d(p) > 0, \end{cases} \quad (8)$$

with n_{imp} as the normal vector n corresponding to the estimated plank state $q_{4,\text{est}}^-$ at the moment of impact as seen in Figure 2. This implies that for all positions p behind the nominal impact line, \bar{p}_d^a is equal to the value of \dot{p}_d^a on the nominal impact line closest to p . This ensures that the controller always has a reference to follow in the ante-impact mode, even when the impact occurs at a different location than expected, which can occur due to uncertainties in the perception of the environment.

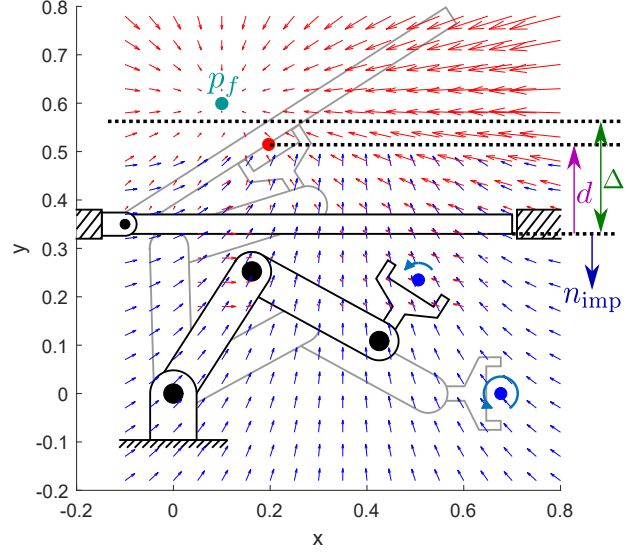


Fig. 2: Depiction of the ante- and post-impact linear velocity references \bar{p}_d^a (blue) and \bar{p}_d^p (red), and ante-impact angular velocity reference $\dot{\theta}_d^a$ (blue) with an initially stationary plank.

2) *Orientation*: To enforce a simultaneous impact with the manipulator, an orientation task is formulated such that the orientation of the end effector θ aligns with the orientation of the surface with which the impact is to take place, in this case described by q_4 . Hence, the desired orientation field is given by

$$\dot{\theta}_d^a(\theta) = K_\theta(q_{4,\text{est}}^- - \theta), \quad (9)$$

with $K_\theta \in \mathbb{R}^+$.

B. Post-impact

As opposed to the ante-impact reference, the post-impact reference only consists of a linear reference velocity field $\bar{p}_d^p(p)$, as the orientation of the manipulator is implicitly described by this position, assuming the manipulator remains in contact with the plank at both contact points. This reference is designed with the goal of reaching the target final position p_f , see Figure 2, while also ensuring that the post-impact velocity is compatible with the ante-impact velocity, resulting in minimal tracking error after the impact, and minimal resulting spikes in the control inputs.

In order to achieve both goals, $\bar{p}_d^p(p)$ is obtained by blending two vector fields. The first vector field, denoted by $\dot{p}_{d,f}^p(p)$, ensures p_f is reached, and is given by

$$\dot{p}_{d,f}^p(p) = k_f(p_f - p). \quad (10)$$

The second vector field, $\bar{p}_{d,\text{imp}}^p(p)$, ensures that the ante- and post-impact references are compatible by linking $\bar{p}_{d,\text{imp}}^p(p)$ to the ante-impact velocity reference ($\bar{p}_d^a(p)$, $\dot{\theta}_d^a(p)$) along the nominal impact line. This is achieved by using the simultaneous impact map (7) to determine the nominal post-impact velocities along the nominal impact line, and extending these velocities along the directions normal to the nominal impact line. The exact formulation of $\bar{p}_{d,\text{imp}}^p(p)$ is

described in Appendix B. Finally, a convex combination of the two reference velocity fields is taken to construct the desired extended post-impact velocity, as

$$\bar{\mathbf{p}}_d^p(\mathbf{p}) = \begin{cases} \bar{\mathbf{p}}_{d,\text{imp}}^p(\mathbf{p}) & \text{if } d(\mathbf{p}) \leq 0, \\ \frac{d(\mathbf{p})}{\Delta} \bar{\mathbf{p}}_{d,\text{imp}}^p(\mathbf{p}) + \left(1 - \frac{d(\mathbf{p})}{\Delta}\right) \dot{\mathbf{p}}_{d,f}^p(\mathbf{p}) & \text{if } 0 < d(\mathbf{p}) < \Delta, \\ \dot{\mathbf{p}}_{d,f}^p(\mathbf{p}) & \text{if } \Delta \leq d(\mathbf{p}), \end{cases} \quad (11)$$

with $\Delta \in \mathbb{R}^+$ as the user-defined width of the band where both $\bar{\mathbf{p}}_{d,\text{imp}}^p$ and $\dot{\mathbf{p}}_{d,f}^p$ contribute to the value of $\bar{\mathbf{p}}_d^p$, as shown in Figure 2. For the nominal motion, this implies that the tracking error will be zero upon switching to the post-impact reference at the moment of impact. Provided that

$$\mathbf{n}_{\text{imp}}^T \bar{\mathbf{p}}_d^p(\mathbf{p}_i) < 0, \forall \mathbf{p}_i \text{ s.t. } 0 \leq d(\mathbf{p}_i) \leq \Delta, \quad (12)$$

and

$$d(\mathbf{p}_f) > \Delta, \quad (13)$$

it can be ensured that following the desired velocity reference $\bar{\mathbf{p}}_d^p$ implies that the manipulator moves away from the nominal impact line until $d(\mathbf{p}) > \Delta$, after which $\bar{\mathbf{p}}_d^p = \dot{\mathbf{p}}_{d,f}^p$, leading to the target position \mathbf{p}_f to be reached in equilibrium.

IV. CONTROL APPROACH

Using the time-invariant reference velocity fields obtained from Section III, we show how to construct a control action for the ante-impact, interim and post-impact mode. In the ante-impact and post-impact mode, the goal is to track the desired reference velocity field, with an additional force task in the post-impact mode. The interim mode is active as long as contact is only partially established. Its main goal is completing the contact without using any velocity error feedback as a result of uncertainties in the contact state. The switching policy is based on detection of the first impact, which activates the interim mode, and then monitoring when full contact is established, which activates the post-impact mode. Each of the modes has a corresponding discrete-time QP controller which is used to obtain a desired joint torque $\boldsymbol{\tau}^*$ to be applied to the robot after every fixed time step Δt .

The control law used for the ante- and post-impact mode described in Section IV-A and IV-C is similar to that described in [13], with the reference explicitly described in time swapped for the time-invariant reference velocity fields described in Section III. As explained in Section I, the interim mode, described in Section IV-B differs significantly from [13], as [13] relies on position feedback in the interim mode, while the approach proposed in this paper does not have an explicit position reference.

A. Ante-impact mode

In the ante-impact mode, the QP optimization variables are given by the torques $\boldsymbol{\tau}$ and the accelerations $\ddot{\mathbf{q}}$. Through position measurements and velocity estimations, \mathbf{q} and $\dot{\mathbf{q}}$ at each time step are assumed to be known. The cost function of the ante-impact QP is selected to be a weighted sum of the costs corresponding to a position and orientation

task, defined such that the ante-impact linear and angular velocity references $\bar{\mathbf{p}}_d^a(\mathbf{p})$ and $\bar{\boldsymbol{\theta}}_d^a(\boldsymbol{\theta})$ defined in Section III-A are followed. The error corresponding to tracking the linear velocity is formulated as

$$\mathbf{e}_p^a = \ddot{\mathbf{p}} - \bar{\mathbf{p}}_d^a(\mathbf{p}) + k_p (\bar{\mathbf{p}}_d^a(\mathbf{p}) - \mathbf{J}_p \dot{\mathbf{q}}), \quad (14)$$

with gain $k_p \in \mathbb{R}^+$ and desired acceleration $\bar{\mathbf{p}}_d^a(\mathbf{p})$ derived from $\bar{\mathbf{p}}_d^p(\mathbf{p})$. Enforcing $\mathbf{e}_p^a = 0$ implies that the desired closed-loop behavior of following the reference $\dot{\mathbf{p}}_d^a(\mathbf{p})$ is indeed imposed. Rewriting the error as

$$\mathbf{e}_p^a = \mathbf{J}_p \ddot{\mathbf{q}} + \boldsymbol{\eta}_p^a, \quad (15)$$

with

$$\boldsymbol{\eta}_p^a = \dot{\mathbf{J}}_p \dot{\mathbf{q}} - \bar{\mathbf{p}}_d^a(\mathbf{p}) - k_p (\bar{\mathbf{p}}_d^a(\mathbf{p}) - \mathbf{J}_p \dot{\mathbf{q}}), \quad (16)$$

and similarly defining the error corresponding to the orientation task with gain k_θ , leads to the weighted cost function

$$E_{\text{ante}} = w_p \left(\ddot{\mathbf{q}}^T \mathbf{J}_p^T \mathbf{J}_p \ddot{\mathbf{q}} + 2 \boldsymbol{\eta}_p^{aT} \mathbf{J}_p \ddot{\mathbf{q}} \right) + w_\theta \left(\ddot{\mathbf{q}}^T \mathbf{J}_\theta^T \mathbf{J}_\theta \ddot{\mathbf{q}} + 2 \boldsymbol{\eta}_\theta^{aT} \mathbf{J}_\theta \ddot{\mathbf{q}} \right) \quad (17)$$

with user-defined task weights $w_p, w_\theta > 0$. Note that the terms independent of the optimization variables have been discarded in (17). Combining this cost function with the equations of motion of the free-moving system, corresponding to (3) with $\boldsymbol{\lambda} = 0$, and a constraint limiting the torque to exceed lower and higher bounds $\underline{\boldsymbol{\tau}}$ and $\bar{\boldsymbol{\tau}}$, respectively, gives the full ante-impact QP as

$$(\ddot{\mathbf{q}}^*, \boldsymbol{\tau}^*) = \min_{\ddot{\mathbf{q}}, \boldsymbol{\tau}} E_{\text{ante}}, \quad (18)$$

s.t.

$$\mathbf{M} \ddot{\mathbf{q}} + \mathbf{h} = \mathbf{S} \boldsymbol{\tau}, \quad (19)$$

$$\underline{\boldsymbol{\tau}} \leq \boldsymbol{\tau} \leq \bar{\boldsymbol{\tau}}. \quad (20)$$

The reference torque $\boldsymbol{\tau}^*$ is subsequently sent to the robot at all times t_k separated by time step Δt , with $\mathbf{q} = \mathbf{q}(t_k)$, $\dot{\mathbf{q}} = \dot{\mathbf{q}}(t_k)$.

B. Interim mode

As advocated earlier, we cannot rely on velocity feedback control using either the ante-, or post-impact velocity reference during the interim mode, as on a real robot the exact contact state is not known. The challenge of this interim mode is hence to formulate a QP tasked with establishing full contact without relying on velocity error feedback.

Our approach aims to achieve this by applying torque as if the system is still in the ante-impact mode, while adding position feedback based on a position error constructed online using the ante-impact velocity reference and the pose detected at the first impact time. For the position, this reference is determined by time integration through

$$\mathbf{p}_d^{\text{int}}(t) = \mathbf{p}(t_{\text{int}}) + \int_{t_{\text{int}}}^t \bar{\mathbf{p}}_d^a(\mathbf{p}) dt, \quad (21)$$

with t_{int} as the moment at which the interim mode starts. This can be iteratively approximated after each time step Δt to obtain

$$\mathbf{p}_d^{\text{int}}(t_k + \Delta t) = \mathbf{p}_d^{\text{int}}(t_k) + \bar{\mathbf{p}}_d^a(\mathbf{p}_d^{\text{int}}(t_k)) \Delta t. \quad (22)$$

To avoid velocity error feedback in the interim mode, $\dot{\mathbf{q}}$ in (15) is replaced by the nominal joint velocity $\dot{\mathbf{q}}_{\text{int}}$ corresponding to the ante-impact velocity references $\bar{\mathbf{p}}_d^a(\mathbf{p})$ and $\bar{\theta}_d^a(\theta)$, given by

$$\dot{\mathbf{q}}_{\text{int}} = [\dot{\mathbf{q}}_{\text{rob,int}}^T \dot{\mathbf{q}}_{4,\text{est}}^-]^T, \quad (23)$$

with

$$\dot{\mathbf{q}}_{\text{rob,int}} := \begin{bmatrix} \mathbf{J}_{p,\text{rob}} \\ \mathbf{J}_{\theta,\text{rob}} \end{bmatrix}^{-1} \begin{bmatrix} \bar{\mathbf{p}}_d^a(\mathbf{p}) \\ \bar{\theta}_d^a(\theta) \end{bmatrix}, \quad (24)$$

and $\dot{\mathbf{q}}_{4,\text{est}}^-$ given by the nominal estimated ante-impact velocity of the plank. Replacing $\dot{\mathbf{q}}$ in (15) by this $\dot{\mathbf{q}}_{\text{int}}$ and adding position feedback using (22), the intermediate mode cost is formulated as

$$\mathbf{e}_p^{\text{int}} = \mathbf{J}_p \ddot{\mathbf{q}} + \boldsymbol{\eta}_p^{\text{int}}, \quad (25)$$

with

$$\boldsymbol{\eta}_p^{\text{int}} = \dot{\mathbf{J}}_{p,\text{int}} \dot{\mathbf{q}}_{\text{int}} - \bar{\mathbf{p}}_d^a(\mathbf{p}) - k_{p,\text{int}} (\mathbf{p}_d^{\text{int}}(t) - \mathbf{p}), \quad (26)$$

$$\dot{\mathbf{J}}_{p,\text{int}} := \sum_{i=1}^4 \frac{\partial \mathbf{J}_p}{\partial q_i} \dot{q}_{\text{int},i}. \quad (27)$$

Please note that the velocity feedback term from (14) has dropped out in (25) since $\dot{\mathbf{p}}_d^a(\mathbf{p}) - \mathbf{J}_p \dot{\mathbf{q}}_{\text{int}} = \mathbf{0}$. Similarly, the cost corresponding to the orientation task can be formulated, leading to the interim mode cost function

$$E_{\text{int}} = w_p \left(\ddot{\mathbf{q}}^T \mathbf{J}_p^T \mathbf{J}_p \ddot{\mathbf{q}} + 2 \boldsymbol{\eta}_p^{\text{int}T} \mathbf{J}_p \ddot{\mathbf{q}} \right) + w_\theta \left(\ddot{\mathbf{q}}^T \mathbf{J}_\theta^T \mathbf{J}_\theta \ddot{\mathbf{q}} + 2 \boldsymbol{\eta}_\theta^{\text{int}T} \mathbf{J}_\theta \ddot{\mathbf{q}} \right). \quad (28)$$

Regarding constraints, the equation of motion constraint (19) is modified, also replacing $\dot{\mathbf{q}}$ by $\dot{\mathbf{q}}_{\text{int}}$, resulting in the interim mode QP formulation

$$(\ddot{\mathbf{q}}^*, \boldsymbol{\tau}^*) = \min_{\ddot{\mathbf{q}}, \boldsymbol{\tau}} E_{\text{int}}, \quad (29)$$

s.t.

$$\mathbf{M} \ddot{\mathbf{q}} + \mathbf{h}(\mathbf{q}, \dot{\mathbf{q}}_{\text{int}}) = \mathbf{S} \boldsymbol{\tau}, \quad (30)$$

$$\underline{\boldsymbol{\tau}} \leq \boldsymbol{\tau} \leq \bar{\boldsymbol{\tau}}. \quad (31)$$

By using a controller that is based on the ante-impact reference, we assure a minimal jump in the desired torque at the moment of the first impact as a result of continuity in the feedforward acceleration $\bar{\mathbf{p}}_d^a$ and $\bar{\theta}_d^a$. Meanwhile, the accumulation of the position feedback error results in a driving force to complete the contact until full contact is established. Stabilization in this mode provided by the dissipating contact dynamics.

C. Post-impact mode

After the final contact state is established, the control input is determined through the post-impact QP, in which it is assumed that both contacts remain closed. While the ante-impact and interim mode did not explicitly take the interaction forces $\boldsymbol{\lambda}$ into account, the post-impact QP does so, and hence, $\boldsymbol{\lambda}$ is included in the optimization variables together with $\ddot{\mathbf{q}}$ and $\boldsymbol{\tau}$.

The QP consists of a task that prescribes the end effector velocity through the reference defined in Section III-B, which

has the same structure as the ante-impact linear velocity task from (15), resulting in the error

$$\mathbf{e}_p^p = \mathbf{J}_p \ddot{\mathbf{q}} + \boldsymbol{\eta}_p^p \quad (32)$$

with

$$\boldsymbol{\eta}_p^p = \dot{\mathbf{J}}_p \dot{\mathbf{q}} - \bar{\mathbf{p}}_d^p(\mathbf{p}) - k_p (\bar{\mathbf{p}}_d^p - \mathbf{J}_p \dot{\mathbf{q}}). \quad (33)$$

As in [13], we add a task encouraging an equal contact force distribution over both contact points, with corresponding weight w_λ , leading to the total cost function

$$E_{\text{post}} = w_p \left(\ddot{\mathbf{q}}^T \mathbf{J}_p^T \mathbf{J}_p \ddot{\mathbf{q}} + 2 \boldsymbol{\eta}_p^{pT} \mathbf{J}_p \ddot{\mathbf{q}} \right) + w_\lambda (\lambda_1 - \lambda_2)^2. \quad (34)$$

For the post-impact constraints, first of all, the constraint prescribing the equations of motion should now include the contact forces, hence (3) is included in the QP. To enforce contact is not lost, we enforce $\boldsymbol{\lambda} \geq \mathbf{0}$, and under the assumption that both contacts are and remain closed, we include a constraint that enforces $\ddot{\gamma} = \mathbf{0}$, resulting in the post-impact QP

$$(\ddot{\mathbf{q}}^*, \boldsymbol{\tau}^*, \boldsymbol{\lambda}^*) = \min_{\ddot{\mathbf{q}}, \boldsymbol{\tau}, \boldsymbol{\lambda}} E_{\text{post}}, \quad (35)$$

s.t.

$$\mathbf{M} \ddot{\mathbf{q}} + \mathbf{h} = \mathbf{S} \boldsymbol{\tau} + \mathbf{J}_N^T \boldsymbol{\lambda}, \quad (36)$$

$$\mathbf{J}_N \ddot{\mathbf{q}} + \dot{\mathbf{J}}_N \dot{\mathbf{q}} = \mathbf{0}, \quad (37)$$

$$\boldsymbol{\lambda} \geq \mathbf{0}, \quad (38)$$

$$\underline{\boldsymbol{\tau}} \leq \boldsymbol{\tau} \leq \bar{\boldsymbol{\tau}}. \quad (39)$$

V. NUMERICAL VALIDATION

To validate the proposed control approach, numerical simulations have been performed¹ using two different robot models. First, simulation results are presented that use the ideal, rigid robot model with rigid contact model as described in Section II. After this, the simulations are repeated for a robot model with flexibility and a low-level torque control loop modeled in its joints, with contact described via a compliant contact model, as was done in [13]. The latter model more closely resembles reality, as flexibility is generally present in, e.g., the drivetrain of robot joints, resulting in oscillations as a result of impacts. These simulations suggest that the developed approach, which uses the assumption of a rigid robot and contact model, is suitable for real-life robot control. We will use both simulation models to compare the proposed control approach against two similar baseline approaches. In the first baseline comparison, referred to as the approach with *no impact map*, we substitute the post-impact reference $\bar{\mathbf{p}}_d^p(\mathbf{p})$ by $\dot{\mathbf{p}}_{d,f}^p(\mathbf{p})$ from (10), which implies that the post-impact reference is not adjusted to the ante-impact reference using the impact map. In the second baseline comparison, referred to as the approach with *no interim mode*, we directly switch to the post-impact control mode upon detection of the first contact, instead of switching to the interim mode first.

¹All simulations can be reproduced using the publicly available Matlab scripts that can be found in <https://gitlab.tue.nl/robotics-lab-public/time-invariant-reference-spreading-for-simultaneous-ir>

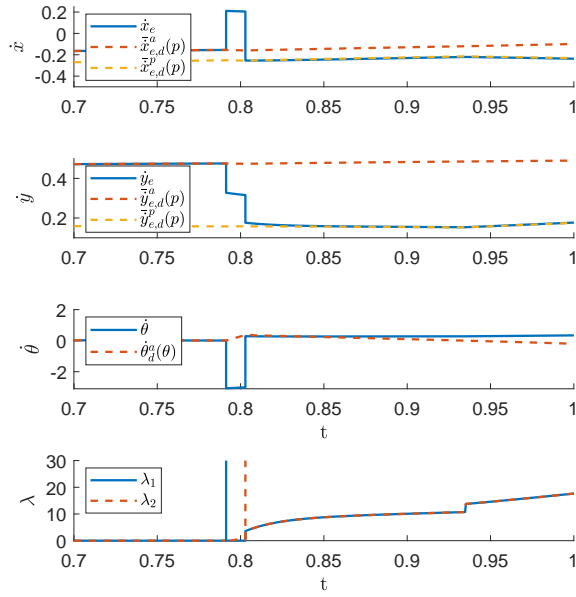


Fig. 3: Cartesian linear and angular end effector velocity and contact forces for the rigid robot model for the proposed control approach.

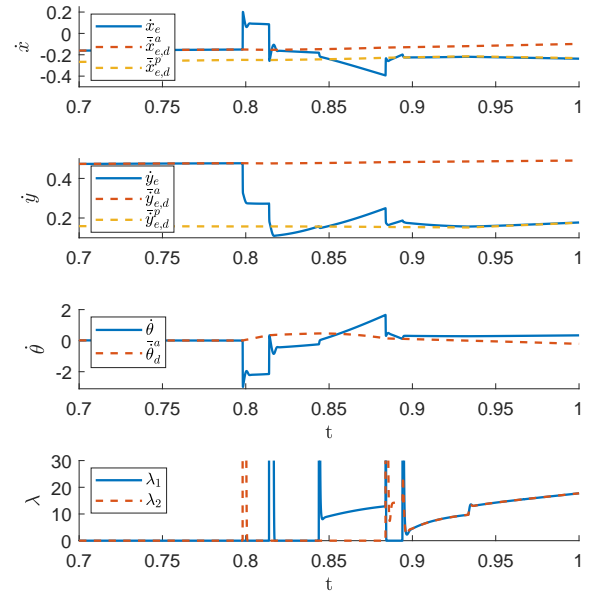


Fig. 5: Cartesian linear and angular end effector velocity and contact forces for the flexible robot model for the proposed control approach.

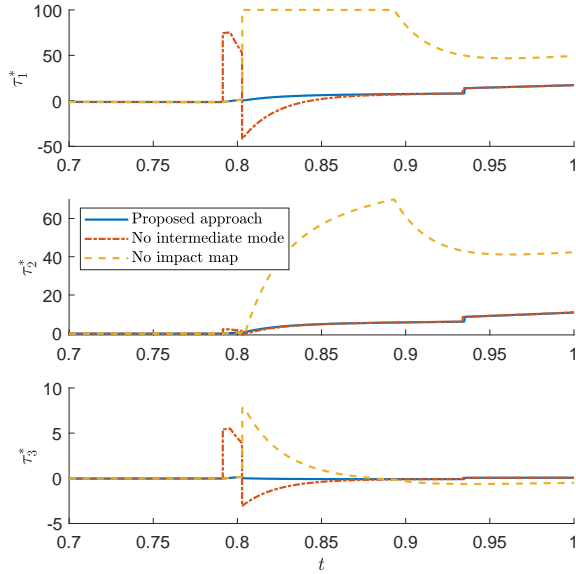


Fig. 4: Commanded torque as simulated using a rigid robot model for different control approaches.

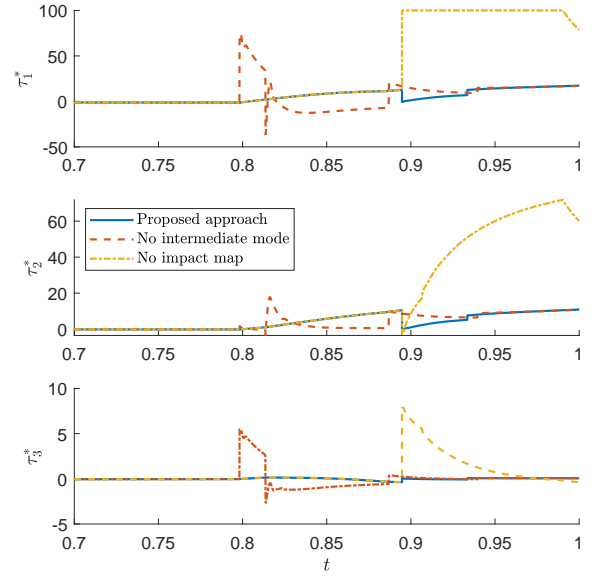


Fig. 6: Commanded torque as simulated using a flexible robot model for different control approaches.

In both simulations, the configuration of the plank q_4 is initialized with an offset compared to the estimated configuration $q_{4,\text{est}}$, which mimics the uncertainty in the environment, and will result in spurious impacts resulting in the system to enter an unexpected contact state.

A. Numerical results with a rigid robot model

First, we will show the results of the simulation that uses a rigid robot model. In Figure 3, the velocities of such simulation with the proposed control approach are presented. It can be observed that two separated impacts occur as a result of the aforementioned initial offset in q_4 and the corresponding misalignment between the end effector and the

impact line at the moment of the first impact. Before the first impact, when the system evolves in the ante-impact mode, the reference $\bar{p}_d^a(\mathbf{p})$ is perfectly followed as expected. After the second impact, when contact is completed and the post-impact mode is entered, it can be observed that the velocity jumps very close to the desired post-impact velocity $\bar{p}_d^p(\mathbf{p})$, which is expected as a result of the reference formulation procedure that takes the impact map and the ante-impact reference explicitly into account. Between the impacts, when the interim mode is active, the velocities, especially \dot{x}_e and $\dot{\theta}$ jump far away from both the corresponding ante-impact and post-impact reference velocities (before jumping back as a

result of the second impact), highlighting that no velocity reference and thus no velocity error can be defined that should be tracked in this mode. After the impacts, the linear velocity reference (note that no reference is prescribed for θ in the post-impact mode) and desired torque task described in Section IV-C are followed as expected.

The effect of applying velocity feedback before full contact is established can be seen in Figure 4, where the approach with no interim mode, in which the post-impact mode is entered upon first contact detection, leads to a sudden increase in input torque τ^* after the first impact occurs. This is caused by a large error between the actual velocity and the post-impact reference velocity. As soon as full contact is established, the torque jumps in opposite direction, to reduce the velocity error caused by the unwanted effort of the controller before full contact is established. This is clearly undesirable behavior, which the proposed approach avoids by the novel interim mode design.

When the post-impact vector field is not constructed by means of the impact map, switching to the post-impact mode after the final impact is detected can lead to a large velocity tracking error, which can subsequently lead to a large input torque τ^* as can be observed from Figure 4, where τ_1^* even reaches the maximum joint torque set in $\bar{\tau}$. This can have an undesired effect, as the sudden extreme jump in τ^* torque can trigger unwanted effects in terms of performance and robustness. As opposed to the two baseline approaches, almost no jump in τ^* occurs upon occurrence of either of the two impacts in the proposed control approach, which highlights the benefits of this approach.

B. Numerical results with a flexible robot model

To validate the effectiveness of the control strategy in a more realistic setting, simulations are also performed on a model of the robotic manipulator from Figure 1 that more closely matches reality, identical to the flexible robot model used for validation in [13]. In this model, the transmission in each joint is modeled as an element with finite stiffness, damping and inertia, and an additional low-level torque control loop is implemented as described in [27], while interaction between the robot and the impacting surface is computed using the compliant exponentially extended Hunt-Crossley contact model from [28].

In Figure 5, the results of simulations with this model are depicted, showing clearly that contact is broken and reinstated several times as a result of the compliant partially elastic contact model, while the flexibility in the joints causes internal vibrations shortly after each impact. However, despite the presence of these vibrations after the initial impact, the desired torque τ^* resulting from the interim mode QP in the proposed approach, seen in Figure 6, does not show any of these vibrations, while sustained contact is still established in the end. This is an additional advantage on top of the benefits described in Section V-A, resulting from the fact that the velocity measurements \dot{q} are not used in the interim mode. This benefit is highlighted when comparing the proposed approach with the baseline approach with no interim mode, where, aside from the jump in τ^* already observed in simulations with the rigid model, the internal

vibrations cause rapid fluctuations in τ^* , which can induce additional undesirable vibrations into the system.

After the interim mode is finished and full contact is established for the proposed approach, a small jump in τ^* can be observed, which is natural given the flexibility in the model that is not explicitly described in the QP controllers. However, when comparing the proposed approach with the approach with no impact map, we can see that the corresponding jump in τ^* is much larger, increasing the likelihood of unwanted effects in terms of performance and robustness.

VI. CONCLUSION

In this paper, a new control framework based on QP control is proposed for robotic manipulators that experience nominally simultaneous impacts. This framework uses separate time-invariant reference fields to prescribe the ante-impact and post-impact tasks, which are matched through an inelastic impact map to minimize the velocity error upon switching. A distinctive feature of the control framework is the additional interim mode, during which position feedback is applied based on time-integration of the ante-impact reference velocity field, in order to establish full sustained contact. Simulation results on a model of a rigid robot with inelastic contact model, and a more realistic flexible robot model with compliant partially elastic contact model, show the effectiveness of the approach. For both models, the motion is successfully executed with accurate tracking of the desired velocity, while minimizing unwanted spikes or fluctuations in the input torque. Future work involves scaling up to a more realistic 3D case and performing a corresponding study on real-life robotic system. This also includes a further study in the moment of switching between control modes based on impact detection. It does, however, not require methodological alterations to the presented approach.

APPENDIX

A. Formulation ante-impact reference

The ante-impact linear velocity reference $\dot{p}_d^a(p)$ is formulated by means of a constant user-defined impact position and velocity p_{imp} and v_{imp} , which indicate the center position of the targeted set of positions on the nominal impact line and the corresponding desired ante-impact velocity. A target position $p_t(p)$ is defined, which is the position at equal distance from p_{imp} as the distance between p and p_{imp} , but aligned to hit p_{imp} with velocity v_{imp} , through

$$p_t(p) = p_{\text{imp}} - \frac{v_{\text{imp}} \|p_{\text{imp}} - p\|_2}{\|v_{\text{imp}}\|_2}. \quad (40)$$

The desired ante-impact velocity $\dot{p}_d^a(p)$ is then formulated as a combination of v_{imp} and a position feedback term using $p_t(p)$, scaled such that for all p , the norm of $\dot{p}_d^a(p)$ is equal to that of v_{imp} . This gives

$$\dot{p}_d^a(p) = \frac{v_{\text{imp}} + \alpha(p_t(p) - p)}{\|v_{\text{imp}} + \alpha(p_t(p) - p)\|_2} \|v_{\text{imp}}\|_2, \quad (41)$$

with $\alpha \in \mathbb{R}^+$ as a user-defined parameter, where increasing α will result in a reference velocity field that steers impacts closer to p_{imp} by taking a wider path towards the nominal impact line.

B. Formulation post-impact reference

To formulate the post-impact reference contribution $\bar{\mathbf{p}}_{d,\text{imp}}^p(\mathbf{p})$ corresponding to the nominal post-impact velocity, we first sample N points that are evenly distributed on the nominal impact line, captured by $\mathbf{p}_{\text{nom},i}$ with $i \in \{1, \dots, N\}$. Assuming that the end effector is perfectly aligned with the impact line ($\theta = q_4$), we can then use inverse kinematics to create a set $\mathbf{q}_{\text{nom},i}$ with the joint configurations corresponding to $\mathbf{p}_{\text{nom},i}$. Using inverse velocity kinematics and assuming to have an estimation of the plank position $\bar{q}_{4,\text{est}}$ and velocity $\dot{\bar{q}}_{4,\text{est}}$ at the moment of impact, we can determine the corresponding nominal ante-impact joint velocities $\dot{\mathbf{q}}_{\text{nom},i}^-$, as

$$\dot{\mathbf{q}}_{\text{nom},i}^- = \begin{bmatrix} \dot{\mathbf{q}}_{\text{rob},\text{nom},i}^T & \dot{\bar{q}}_{4,\text{est}} \end{bmatrix}^T, \quad (42)$$

with

$$\dot{\mathbf{q}}_{\text{rob},\text{nom},i}^- = \begin{bmatrix} \mathbf{J}_{p,\text{rob}}(\mathbf{q}_{\text{nom},i}) \\ \mathbf{J}_{\theta,\text{rob}}(\mathbf{q}_{\text{nom},i}) \end{bmatrix}^{-1} \begin{bmatrix} \bar{\mathbf{p}}_d^a(\mathbf{p}_{\text{nom},i}) \\ \theta_d^a(\bar{q}_{4,\text{est}}) \end{bmatrix}. \quad (43)$$

Using the impact map (7), we can determine the corresponding post-impact joint velocities $\dot{\mathbf{q}}_{\text{nom},i}^+$, which can be translated to velocities in operational space via

$$\dot{\mathbf{p}}_{d,\text{imp}}^p(\mathbf{p}_{\text{nom},i}) = \mathbf{J}_p(\mathbf{q}_{\text{nom},i}) \dot{\mathbf{q}}_{\text{nom},i}^+. \quad (44)$$

To ensure that we can compute $\dot{\mathbf{p}}_{d,\text{imp}}^p(\mathbf{p})$ for each position without having to recompute the inverse kinematics and impact map, we interpolate between the values of $\dot{\mathbf{p}}_{d,\text{imp}}^p(\mathbf{p}_{\text{nom},i})$ using radial basis function interpolation. Finally, we extend this velocity field in the directions normal to the nominal impact line in similar fashion to the extension in (8), to come to the expression of $\bar{\mathbf{p}}_{d,\text{imp}}^p(\mathbf{p})$ as

$$\bar{\mathbf{p}}_{d,\text{imp}}^p(\mathbf{p}) := \dot{\mathbf{p}}_{d,\text{imp}}^p(\mathbf{p} + d(\mathbf{p})\mathbf{n}_{\text{imp}}), \quad (45)$$

recalling that $d(\mathbf{p})$ represents the smallest distance from \mathbf{p} to the nominal impact line, while \mathbf{n}_{imp} represents the vector normal to the nominal impact line, as seen in Figure 2.

ACKNOWLEDGMENT

This work was partially supported by the Research Project I.A.M. through the European Union H2020 program under GA 871899.

REFERENCES

- [1] R. Tajima, D. Honda, and K. Suga, "Fast Running Experiments Involving a Humanoid Robot," in *International Conference on Robotics and Automation*, pp. 1571–1576, IEEE, 2009.
- [2] T. Stouraitis, L. Yan, J. Moura, M. Gienger, and S. Vijayakumar, "Multi-mode Trajectory Optimization for Impact-aware Manipulation," in *International Conference on Intelligent Robots and Systems (IROS)*, pp. 9425–9432, IEEE, 2020.
- [3] J. J. Biemond, N. van de Wouw, W. P. H. Heemels, and H. Nijmeijer, "Tracking Control for Hybrid Systems With State-Triggered Jumps," *IEEE Transactions on Automatic Control*, vol. 58, no. 4, pp. 876–890, 2013.
- [4] R. I. Leine and N. van de Wouw, *Stability and Convergence of Mechanical Systems with Unilateral Constraints*, vol. 36 of *Lecture Notes in Applied and Computational Mechanics*. Springer Berlin Heidelberg, 2008.
- [5] K. Benali, J.-F. Brethé, F. Guérin, and M. Gorka, "Dual Arm Robot Manipulator for Grasping Boxes of Different Dimensions in a Logistics Warehouse," in *International Conference on Industrial Technology*, pp. 147–152, IEEE, 2018.

- [6] W. Yang and M. Posa, "Impact Invariant Control with Applications to Bipedal Locomotion," in *International Conference on Intelligent Robots and Systems (IROS)*, pp. 5128–5135, IEEE, 2021.
- [7] I. C. Morărescu and B. Brogliato, "Trajectory Tracking Control of Multiconstraint Complementarity Lagrangian Systems," *IEEE Transactions on Automatic Control*, vol. 55, no. 6, pp. 1300–1313, 2010.
- [8] A. Saccon, N. van de Wouw, and H. Nijmeijer, "Sensitivity analysis of hybrid systems with state jumps with application to trajectory tracking," in *Conference on Decision and Control*, pp. 3065–3070, IEEE, 2014.
- [9] M. Rijnen, A. Saccon, and H. Nijmeijer, "On Optimal Trajectory Tracking for Mechanical Systems with Unilateral Constraints," in *Conference on Decision and Control*, pp. 2561–2566, IEEE, 2015.
- [10] M. Rijnen, B. Biemond, N. van de Wouw, A. Saccon, and H. Nijmeijer, "Hybrid Systems with State-Triggered Jumps: Sensitivity-Based Stability Analysis with Application to Trajectory Tracking," *IEEE Transactions on Automatic Control*, vol. 65, no. 11, pp. 4568–4583, 2019.
- [11] M. Rijnen, A. Saccon, and H. Nijmeijer, "Reference Spreading: Tracking Performance for Impact Trajectories of a 1DoF Setup," *IEEE Transactions on Control Systems Technology*, vol. 28, no. 3, pp. 1124–1131, 2020.
- [12] M. Rijnen, H. L. Chen, N. van de Wouw, A. Saccon, and H. Nijmeijer, "Sensitivity analysis for trajectories of nonsmooth mechanical systems with simultaneous impacts: A hybrid systems perspective," in *American Control Conference*, pp. 3623–3629, IEEE, 2019.
- [13] J. J. van Steen, N. van de Wouw, and A. Saccon, "Robot Control for Simultaneous Impact Tasks via QP Based Reference Spreading," 2022.
- [14] J. Hauser and R. Hindman, "Maneuver Regulation from Trajectory Tracking: Feedback Linearizable Systems," in *IFAC Symposium on Nonlinear Control System Design*, vol. 28, pp. 595–600, 1995.
- [15] A. P. Aguiar, J. P. Hespanha, and P. V. Kokotović, "Path-following for nonminimum phase systems removes performance limitations," *IEEE Transactions on Automatic Control*, vol. 50, no. 2, pp. 234–239, 2005.
- [16] S. M. Khansari-Zadeh and A. Billard, "A dynamical system approach to realtime obstacle avoidance," *Autonomous Robots*, vol. 32, no. 4, pp. 433–454, 2012.
- [17] S. M. Salehian and A. Billard, "A Dynamical-System-Based Approach for Controlling Robotic Manipulators During Noncontact/Contact Transitions," *IEEE Robotics and Automation Letters*, vol. 3, pp. 2738–2745, oct 2018.
- [18] S. M. Khansari-Zadeh, K. Kronander, and A. Billard, "Learning to Play Minigolf: A Dynamical System-Based Approach," *Advanced Robotics*, vol. 26, no. 17, pp. 1967–1993, 2012.
- [19] H. Khurana, M. Bombile, and A. Billard, "Learning to Hit: A statistical Dynamical System based approach," in *International Conference on Intelligent Robots and Systems*, pp. 9415–9421, IEEE, 2021.
- [20] K. Bouyarmane, K. Chappellet, J. Vaillant, and A. Kheddar, "Quadratic Programming for Multirobot and Task-Space Force Control," *IEEE Transactions on Robotics*, vol. 35, no. 1, pp. 64–77, 2019.
- [21] J. Salini, S. Barthélemy, and P. Bidaud, "LQP-Based Controller Design for Humanoid Whole-Body Motion," in *Advances in Robot Kinematics: Motion in Man and Machine*, pp. 177–184, Springer, 2010.
- [22] A. Escande, N. Mansard, and P.-B. Wieber, "Hierarchical quadratic programming: Fast online humanoid-robot motion generation," *The International Journal of Robotics Research*, vol. 33, no. 7, pp. 1006–1028, 2014.
- [23] N. Dehio and A. Kheddar, "Robot-Safe Impacts with Soft Contacts Based on Learned Deformations," in *International Conference on Robotics and Automation*, pp. 1357–1363, IEEE, 2021.
- [24] Y. Wang and A. Kheddar, "Impact-Friendly Robust Control Design with Task-Space Quadratic Optimization," in *Proceedings of Robotics: Science and Systems*, 2019.
- [25] B. Brogliato, *Nonsmooth Mechanics*. Communications and Control Engineering, Springer International Publishing, 3rd ed., 2016.
- [26] C. Glocker, "An Introduction to Impacts," in *Nonsmooth Mechanics of Solids, CISM Courses and Lectures*, vol. 485, pp. 45–101, Springer, Vienna, 2006.
- [27] A. Albu-Schäffer, C. Ott, and G. Hirzinger, "A Unified Passivity-based Control Framework for Position, Torque and Impedance Control of Flexible Joint Robots," *The International Journal of Robotics Research*, vol. 26, no. 1, pp. 23–39, 2007.
- [28] A. S. Carvalho and J. M. Martins, "Exact restitution and generalizations for the Hunt – Crossley contact model," *Mechanism and Machine Theory*, vol. 139, pp. 174–194, 2019.